

A Bayesian framework for spectral reprojection ^{*†}

Tongtong Li[‡] and Anne Gelb[†]

Abstract. Fourier partial sum approximations yield exponential accuracy for smooth and periodic functions, but produce the infamous Gibbs phenomenon for non-periodic ones. Spectral reprojection resolves the Gibbs phenomenon by projecting the Fourier partial sum onto a Gibbs complementary basis, often prescribed as the Gegenbauer polynomials. Noise in the Fourier data and the Runge phenomenon both degrade the quality of the Gegenbauer reconstruction solution, however. Motivated by its theoretical convergence properties, this paper proposes a new Bayesian framework for spectral reprojection, which allows a greater understanding of the impact of noise on the reprojection method from a statistical point of view. We are also able to improve the robustness with respect to the Gegenbauer polynomials parameters. Finally, the framework provides a mechanism to quantify the uncertainty of the solution estimate.

Key words. Bayesian inference method; spectral reprojection; noisy Fourier data; Gibbs phenomenon; Gegenbauer polynomials; uncertainty quantification

AMS subject classifications (2020). 41A10, 42C05, 62F15, 65T40

DOI. Not yet assigned

1. Introduction. Fourier samples model data acquisitions in applications such as magnetic resonance imaging (MRI) and synthetic aperture radar (SAR). Indeed, recovering images from either MRI k -space data or SAR phase history data most often involves recasting the problem as a linear inverse problem with the forward operator given by the discrete (non-uniform) Fourier transform (DFT) matrix (see e.g. [3, 4, 23, 29, 35]). Compressive sensing (CS) algorithms that promote sparse solutions in a known sparse domain [6, 16, 17, 33] have become increasingly widespread in providing point estimate image recoveries. More recently, Bayesian inference methods have been developed to also quantify the uncertainty of the estimate.

This investigation develops a new Bayesian framework for recovering smooth but non-periodic functions from given noisy Fourier data. Uncertainty quantification can also be achieved when the hyperparameters in the posterior density function are fixed. Importantly, however, rather than use the often employed *sparse prior* (or sparse penalty term in CS), here we construct a prior based on *spectral reprojection* [26, 25].

The spectral reprojection method is a *forward* approach designed to *reproject* the observable Fourier data onto a Gibbs complementary basis. It is sometimes referred to as Gegenbauer reconstruction when the Gibbs complementary basis is comprised of Gegenbauer polynomials. The reprojection eliminates the Gibbs phenomenon and restores the exponential convergence (hence the use of *spectral* in its name) in the maximum norm. For self-containment, we summarize spectral reprojection in [subsection 2.2](#).

Although Gegenbauer reconstruction has been successfully used in applications where the observable Fourier data have complex additive Gaussian noise of mean zero [3, 42], it was also demonstrated in [5] that while the estimator is unbiased, its variance is spatially dependent. Nevertheless, theoretical results in the seminal work [26] provide key insights that inspire us to develop a new Bayesian inference method

^{*}This work is partially supported by the NSF grant DMS #1912685, AFOSR grant #F9550-22-1-0411, DOE ASCR #DE-AC05-000R22725, and DOD ONR MURI grant #N00014-20-1-2595.

[†]June 25, 2024

[‡]Department of Mathematics, Dartmouth College, Hanover, NH 03755, USA (tongtong.li@dartmouth.edu, tongtong.li@umbc.edu, orcid.org/0000-0002-7664-4764 and Anne.E.Gelb@Dartmouth.edu, orcid.org/0000-0002-9219-4572)

for the corresponding *inverse* problem. Namely, the derivation of the error terms in the exponential convergence proof naturally motivates the choices of the likelihood and prior terms in the Bayesian method. In particular, the prior used for the construction of the posterior should be designed to favor solutions whose orthogonal polynomial partial sum expansion yields good approximations. Such an assumption is consistent for recovering (discretized) functions that are smooth but not periodic, and is arguably more appropriate than using a sparsifying operator such as first order differencing, which by design assumes that the underlying function is piecewise constant, or Tikhonov regularization, which is even more restrictive. Moreover, when coupled with the likelihood term, the common kernel condition [31] is automatically satisfied so that a unique minimum for the corresponding *maximum a posteriori* (MAP) estimate may be obtained. We call this approach the *Bayesian spectral reprojection* (BSR) method, and its point estimate solution, which is consistent with Gegenbauer reconstruction, is the MAP estimate of the corresponding posterior density and is determined through optimization. As already noted, we are also able to provide uncertainty quantification for fixed hyperparameters.

We further propose a *generalized* Bayesian spectral reprojection (GBSR) method, which modifies the BSR by formulating the likelihood so that the observables are not first transformed to the Gibbs complementary basis. Rather, we directly use the observable Fourier data for this purpose. Removing this restriction allows us to explore a larger space that still assumes that the function is well-approximated by the Gegenbauer partial sum expansion, but also seeks a good fit to the observable data. As our numerical results demonstrate, the point estimate obtained for GBSR is more robust in low SNR environments to different parameter choices. It is also possible to quantify the uncertainty when the posterior density function uses fixed hyperparameters.

Paper organization. The rest of this paper is organized as follows. [Section 2](#) describes the underlying problem and summarizes the spectral reprojection method [25]. The problem is then discretized in [Section 3](#) to enable the Bayesian approach used in [Section 4](#). There we describe how the theoretical results proving exponential convergence for spectral reprojection inspire the construction of a new prior, leading to the Bayesian spectral reprojection (BSR) method. These ideas are then modified in [Section 5](#) for the *generalized* Bayesian spectral reprojection (GBSR) method. Numerical examples in [Section 6](#) show the efficacy of our new methods for recovering 1D smooth functions from noisy Fourier data. [Section 7](#) provides some concluding remarks.

2. Preliminaries. Let f be a real-valued analytic L^2 integrable function on $[-1, 1]$. We are given its first N (for convenience we choose N to be even) noisy Fourier measurements $\widehat{\mathbf{b}} \in \mathbb{C}^N$ with components

$$(2.1) \quad \widehat{b}_k = \widehat{f}_k + \widehat{\epsilon}_k, \quad k = -\frac{N}{2}, \dots, \frac{N}{2} - 1,$$

where

$$(2.2) \quad \widehat{f}_k = \frac{1}{2} \int_{-1}^1 f(x) e^{-ik\pi x} dx,$$

and the components $\widehat{\epsilon}_k \sim \mathcal{CN}(0, \alpha^{-1})$ of $\widehat{\epsilon} \in \mathbb{C}^N$ each follows a circularly-symmetric complex normal distribution with unknown variance $\alpha^{-1} > 0$. The noiseless Fourier partial sum approximation

$$(2.3) \quad S_N f(x) = \sum_{k=-\frac{N}{2}}^{\frac{N}{2}-1} \widehat{f}_k e^{ik\pi x}$$

yields the infamous Gibbs phenomenon for non-periodic f [24], notably manifested by the spurious oscillations at the boundaries $x = \pm 1$ as well as an overall reduced order of convergence away from

the boundaries. We note that the Gibbs phenomenon also occurs whenever f is piecewise smooth with spurious oscillations forming near internal discontinuity locations. When these locations are known in advance the techniques introduced in this investigation can be straightforwardly adapted via linear transformation. When they are unknown, methods such as those in [19, 39] can be first applied to find them. Thus to simplify our presentation we will only consider non-periodic analytic L^2 integrable functions on $[-1, 1]$.

2.1. Resolution of the Gibbs phenomenon. The Gibbs phenomenon has been extensively studied for a variety of applications. While the purpose of this investigation is neither to survey nor compare the myriad techniques developed to resolve it, we describe a few well-known methods for context.

Spectral filters (see e.g. [41]) provide the most straightforward and cost efficient approach for mitigating the Gibbs phenomenon, but cause fine details of the solution to be “smoothed out” at the boundaries of non-periodic smooth functions. Another forward method is *spectral reprojection*, first introduced in [26], which can more sharply resolve the approximation by first reprojecting (2.3) into a more suitable basis. The inverse polynomial reconstruction method in [37] and least squares method developed in [2] (which is designed for general samples in a separable Hilbert space) can sometimes better resolve the Gibbs phenomenon, but there is a trade-off between stability and increased points-per-wave requirement. Convex optimization approaches using ℓ_1 regularization, commonly referred to as compressive sensing algorithms (e.g. [6]) have also been used successfully. Each of these methods requires parameter tuning, which becomes increasingly difficult as more noise is prevalent in the data. Moreover, they are not designed to quantify the uncertainty of the solution. This is particularly problematic since different parameter choices can sometimes lead to wildly different approximations. Finally we mention the statistical filter method developed in [38] which constructs the approximation from the given Fourier data by minimizing the error over a set of possible reconstructions. Although the approach is Bayesian, it does not provide any uncertainty quantification. Our goal here is therefore to develop a Bayesian approach that (1) accurately approximates a smooth but non-periodic function in $[-1, 1]$ on a chosen set of pixels given a finite number of its noisy Fourier coefficients, and (2) quantifies the uncertainty in the approximation.

2.2. Spectral reprojection. In a nutshell, spectral reprojection *reprojects* $S_N f$ in (2.3) onto a more suitable *Gibbs complementary* basis. Under certain parameter constraints, the Gegenbauer polynomials serve as a reprojection basis that ensures exponential accuracy in the maximum norm *without* significantly increasing the points-per-wave requirement. These constraints eliminate both Chebyshev and Legendre polynomials as suitable.¹ Below we provide a brief synopsis as it pertains to our investigation. An in depth review of spectral reprojection and its convergence analysis may be found in [25].

In order to achieve exponential accuracy, the reprojection basis must have the property that the high modes of the Fourier basis have exponentially small projections onto its low modes. Let the polynomial basis $\{\psi_l^\lambda\}$, with the parameter $\lambda \in \mathbb{R}^+$ corresponding to a prescribed weight function w_λ and index $l \in \mathbb{Z}^+ \cup \{0\}$ corresponding to its degree, be such a basis. The m th-degree polynomial approximation of a function f using $\{\psi_l^\lambda\}_{l=0}^m$ is given by

$$(2.4) \quad P_m^\lambda f(x) := \sum_{l=0}^m \hat{f}_l^\lambda \psi_l^\lambda(x).$$

¹Other Gibbs complementary bases, such as the Freud polynomials, may be more robust [20]. As here we are focused on using a Bayesian framework, the closed form solutions provided by the Gegenbauer polynomials makes the analysis and implementation more convenient.

To determine the coefficients \widehat{f}_l^λ , consider the standard definition for a weighted inner product with respect to the prescribed weight function w_λ

$$(2.5) \quad \langle f, g \rangle_{w_\lambda} = \int_{-1}^1 w_\lambda(x) f(x) g(x) dx.$$

We choose $\{\psi_l^\lambda\}_{l=0}^m$ to be orthogonal with respect to w_λ so that

$$(2.6) \quad \langle \psi_l^\lambda, \psi_{l'}^\lambda \rangle_{w_\lambda} = \int_{-1}^1 w_\lambda(x) \psi_l^\lambda(x) \psi_{l'}^\lambda(x) dx = \begin{cases} \|\psi_l^\lambda\|_{w_\lambda}^2 & := h_l^\lambda \quad \text{if } l = l', \\ 0 & \text{otherwise,} \end{cases}$$

where for ease of notation we have defined $h_l^\lambda = \|\psi_l^\lambda\|_{w_\lambda}^2$. Hence by construction the coefficients \widehat{f}_l^λ in (2.4) are determined as

$$(2.7) \quad \widehat{f}_l^\lambda = \frac{\langle f, \psi_l^\lambda \rangle_{w_\lambda}}{\|\psi_l^\lambda\|_{w_\lambda}^2} = \frac{1}{h_l^\lambda} \int_{-1}^1 w_\lambda(x) f(x) \psi_l^\lambda(x) dx.$$

An admissible Gibbs complementary basis must first and foremost yield exponential convergence (see e.g. [10, 28]) in the maximum norm as a partial sum expansion for analytic L^2 integrable $f \in L^2[-1, 1]$. That is,

$$(2.8) \quad \max_{-1 \leq x \leq 1} |f(x) - P_m^\lambda f(x)| \leq \text{Const}_1 \cdot e^{-mr}$$

for $m \gg 1$ and $r > 0$. The significance of the *reprojection* method lies in the observation that f in (2.4) can be replaced by its N -term Fourier expansion $S_N f$ in (2.3) yielding

$$(2.9) \quad P_m^\lambda S_N f(x) := \sum_{l=0}^m \widehat{g}_l^\lambda \psi_l^\lambda(x)$$

where

$$\widehat{g}_l^\lambda = \frac{\langle S_N f, \psi_l^\lambda \rangle_{w_\lambda}}{\|\psi_l^\lambda\|_{w_\lambda}^2} = \frac{1}{h_l^\lambda} \int_{-1}^1 w_\lambda(x) S_N f(x) \psi_l^\lambda(x) dx,$$

while still retaining exponential reconstruction accuracy in the maximum norm on $[-1, 1]$. That is,

$$(2.10) \quad \max_{-1 \leq x \leq 1} |f(x) - P_m^\lambda S_N f(x)| \leq \text{Const}_2 \cdot e^{-mp},$$

for $m \gg 1$ and $p > 0$. Satisfying (2.10) requires that $m = \kappa N$ for some admissible $\kappa < 1$ (see Theorem 2.1 below). This is a profound statement which says that a poorly converging N -term Fourier expansion contains sufficient information to recover and approximate the function with exponential accuracy. The form of (2.9) gives the method its name – the Fourier partial sum approximation is *reprojected* to a Gibbs complementary basis yielding *spectral* accuracy.

2.3. Gegenbauer polynomials. Mainly due to straightforward analysis and convenient closed form equations that can be used directly in numerical implementation, the most commonly employed Gibbs complementary basis is the family of Gegenbauer polynomials, $\{C_l^\lambda(x)\}_{l=0}^m$. We use them here as well, and note that for robustness purposes, in some cases it might be beneficial to instead use the Freud polynomials [20] (see Remark 6.1). We also point out that there is no inherent constraint that the reprojection basis need be polynomials. We now proceed to provide the definition of the Gegenbauer polynomials. As in [26], we rely on [7] for several of the corresponding explicit formulae.

Definition 2.1. *The Gegenbauer polynomial $C_l^\lambda(x)$, $\lambda \geq 0$, is the polynomial of degree l that satisfies*

$$\int_{-1}^1 w_\lambda(x) C_k^\lambda(x) C_l^\lambda(x) dx = 0, \quad k \neq l,$$

where $w_\lambda(x) = (1 - x^2)^{\lambda - \frac{1}{2}}$ is the corresponding weight function. The normalizing term h_l^λ in (2.7) is explicitly given by

$$(2.11) \quad h_l^\lambda = \pi^{\frac{1}{2}} C_l^\lambda(1) \frac{\Gamma(\lambda + \frac{1}{2})}{\Gamma(\lambda)\Gamma(l + \lambda)}.$$

Here $C_l^\lambda(1) = \frac{\Gamma(l+2\lambda)}{l!\Gamma(2\lambda)}$ and $\Gamma(\lambda)$ denotes the usual gamma function.

By substituting $C_l^\lambda(x)$ into (2.4), we obtain the Gegenbauer partial sum expansion

$$(2.12) \quad P_m^\lambda f(x) = \sum_{l=0}^m \widehat{f}_l^\lambda C_l^\lambda(x),$$

with Gegenbauer coefficients in (2.7) provided by

$$(2.13) \quad \widehat{f}_l^\lambda = \frac{1}{h_l^\lambda} \int_{-1}^1 (1 - x^2)^{\lambda - \frac{1}{2}} f(x) C_l^\lambda(x) dx.$$

Note that (2.12) converges exponentially in the sense of (2.8) for f analytic in $[-1, 1]$ and $\lambda \geq 0$ [10, 28]. In particular, Chebyshev ($\lambda = 0$) and Legendre ($\lambda = \frac{1}{2}$) are classical examples of Gegenbauer polynomials.

Because it inspires the development of our new Bayesian approach to spectral reprojection, we quote the main theorem in [26, Theorem 5.1]:

Theorem 2.1 (Removal of the Gibbs Phenomenon). *Consider an analytic and non-periodic function $f(x)$ on $[-1, 1]$, satisfying*

$$(2.14) \quad \max_{-1 \leq x \leq 1} \left| \frac{d^k f}{dx^k}(x) \right| \leq C(\rho) \frac{k!}{\rho^k}, \quad \rho \geq 1.$$

Assume that the first N Fourier coefficients in (2.2) are known. Let \widehat{g}_l^λ , $0 \leq l \leq m$, be the Gegenbauer reprojection coefficients in (2.9)

$$(2.15) \quad \widehat{g}_l^\lambda = \frac{1}{h_l^\lambda} \int_{-1}^1 (1 - x^2)^{\lambda - \frac{1}{2}} S_N f(x) C_l^\lambda(x) dx = \delta_{0l} \widehat{f}_0 + \Gamma(\lambda) i^l (l + \lambda) \sum_{k=-\frac{N}{2}}^{\frac{N}{2}-1} J_{l+\lambda}(\pi k) \left(\frac{2}{\pi k} \right)^\lambda \widehat{f}_k,$$

where $S_N f$ is the Fourier partial sum given by (2.3), δ_{0l} is the Kronecker delta function, $\Gamma(\lambda)$ denotes the usual gamma function, and $J_{l+\lambda}(\pi k)$ is the Bessel function of the first kind.² Then, for $\lambda = m = \kappa N$ where $\kappa < \frac{\pi e}{27}$, we have

$$(2.16) \quad \max_{-1 \leq x \leq 1} \left| f(x) - \sum_{l=0}^m \widehat{g}_l^\lambda C_l^\lambda(x) \right| \leq A_D N^2 q_D^N + A_R q_R^N,$$

where

$$q_D = \left(\frac{27\kappa}{\pi e} \right)^\kappa, \quad q_R = \left(\frac{27}{32\rho} \right)^\kappa.$$

The proof found in [26, 25] makes use of the explicit form in (2.15) and follows the triangular inequality

$$(2.17) \quad \begin{aligned} \max_{-1 \leq x \leq 1} \left| f(x) - \sum_{l=0}^m \widehat{g}_l^\lambda C_l^\lambda(x) \right| &\leq \max_{-1 \leq x \leq 1} \left| \sum_{l=0}^m \widehat{f}_l^\lambda C_l^\lambda(x) - \sum_{l=0}^m \widehat{g}_l^\lambda C_l^\lambda(x) \right| \\ &+ \max_{-1 \leq x \leq 1} \left| f(x) - \sum_{l=0}^m \widehat{f}_l^\lambda C_l^\lambda(x) \right| \\ &= \|E_D\|_\infty + \|E_R\|_\infty \\ &\leq A_D N^2 q_D^N + A_R q_R^N. \end{aligned}$$

The first term, called the *truncation error* in [26, 25], is a measure of how well the projected data fits the true data (hence we refer to this term as the *data error* and use E_D) in the Gibbs complementary basis (here the Gegenbauer polynomials with $\lambda = \kappa N$). The regularization error (E_R) measures how accurate the m th-degree approximation is in the Gibbs complementary basis given the true coefficients $\{\widehat{f}_l^\lambda\}_{l=0}^m$. Importantly, the error bound is provided in the *maximum* norm, proving that the spectral reprojection method in (2.9) using the Gegenbauer polynomials as the reprojection basis with appropriate λ and m truly resolves the Gibbs phenomenon. We also note that referring to the two error components as respectively the data and regularization errors provides some intuition for the Bayesian approach we adopt in Section 4.

To summarize, given the first N Fourier coefficients (2.2) of a non-periodic analytic function on $[-1, 1]$, Theorem 2.1 says that the Gegenbauer polynomials can be used as the Gibbs complementary basis in (2.9), with coefficients $\{\widehat{g}_l^\lambda\}_{l=0}^m$ defined in (2.15). This yields the celebrated *Gegenbauer reconstruction method*

$$(2.18) \quad f_{m,N}^\lambda(x) := P_m^\lambda S_N f(x) = \sum_{l=0}^m \widehat{g}_l^\lambda C_l^\lambda(x),$$

which converges exponentially to f for any $x \in [-1, 1]$ in the maximum norm.

Remark 2.1. *Theorem 2.1 does not suggest that $m = \lambda$, only that they both grow linearly with N . Indeed, while the regularization error E_R decreases with larger m , the data error E_D increases. Larger λ decreases E_D , but creates a narrower weight function, causing the approximation to be more extrapolatory. A more thorough investigation for optimizing these parameters, based on the underlying regularity of f , can be found in [18]. Moreover, the theorem rules out using Legendre ($\lambda = \frac{1}{2}$) or Chebyshev*

²The explicit formula in (2.15) is discussed in [26] and results from properties of orthogonal polynomials, see e.g. [1].

polynomials ($\lambda = 0$), since λ must grow linearly with N to ensure small E_D . Thus we see that although they both yield exponentially convergent approximations for E_R according to (2.8), they do not qualify as admissible Gibbs complementary bases. Finally, it is important to note that [Theorem 2.1](#) does not account for the additive Gaussian noise in (2.1), and while the general estimate still holds [5], parameter optimization is less clear. This will be further discussed in [Remark 4.2](#), [Remark 4.3](#), and [subsection 6.2](#).

Although (2.18) can approximate f at any point location x in $[-1, 1]$, for simplicity in this investigation we discretize the spatial domain uniformly using the same number of points as given Fourier data, so that

$$(2.19) \quad x_j = -1 + \frac{2(j-1)}{N}, \quad j = 1, \dots, N.$$

Uniform discretization is also desirable as it is standard for pixelated images. We then seek to recover an approximation to the vectorized solution $\mathbf{f} \in \mathbb{R}^N$, where each component of \mathbf{f} is given by $f_j = f(x_j)$, $j = 1, \dots, N$. [Algorithm 2.1](#) describes how to approximate f at the prescribed gridpoints (2.19) satisfying the conditions in (2.14) given its noisy Fourier coefficients (2.1) using the blueprint provided by [Theorem 2.1](#). Results for the *noiseless* case first described in [26] are displayed in [Figure 6.2](#).

Algorithm 2.1 Gegenbauer reprojection from noisy Fourier data

Input Data vector $\widehat{\mathbf{b}} = \{\widehat{b}_k\}_{k=-\frac{N}{2}}^{\frac{N}{2}-1} \in \mathbb{C}^N$ in (2.1), choices for $\lambda = \kappa_1 N$ and $m = \kappa_2 N$, $0 < \kappa_1, \kappa_2 < 1$, and grid points x_j , $j = 1, \dots, N$.

Output Approximation $f_{m,N}^\lambda(x_j)$, $j = 1, \dots, N$.

Step 1. Calculate the approximate Gegenbauer coefficients as

$$(2.20) \quad \widehat{g}_l^\lambda = \delta_{0l} \widehat{b}_0 + \Gamma(\lambda) i^l (l + \lambda) \sum_{k=-\frac{N}{2}}^{\frac{N}{2}-1} J_{l+\lambda}(\pi k) \left(\frac{2}{\pi k}\right)^\lambda \widehat{b}_k, \quad l = 0, \dots, m,$$

where $J_\nu(\cdot)$ is the Bessel function of the first kind.

Step 2. Construct the Gegenbauer partial sum approximation

$$(2.21) \quad f_{m,N}^\lambda(x_j) = \sum_{l=0}^m \widehat{g}_l^\lambda C_l^\lambda(x_j), \quad j = 1, \dots, N.$$

3. Model discretization. Since we will be formulating our problem as a discrete linear inverse problem, we now describe how the results in [Section 2](#) can be discretized and expressed using matrix-vector notation. Following standard terminology for recovery problems, we will refer to $\mathbf{f} = \{f(x_j)\}_{j=1}^N \in \mathbb{R}^N$ as the underlying signal of interest.

Recall that for uniform grid points (2.19), the composite trapezoidal rule can be used to approximate $\widehat{\mathbf{f}} = \{\widehat{f}_k\}_{k=-\frac{N}{2}}^{\frac{N}{2}-1}$ in (2.2) as

$$(3.1) \quad \widetilde{f}_k = \frac{1}{N} \sum_{j=1}^N f(x_j) e^{-ik\pi x_j}, \quad -\frac{N}{2} \leq k \leq \frac{N}{2} - 1,$$

which we write in matrix-vector form as

$$(3.2) \quad \widetilde{\mathbf{f}} = \mathbf{F}\mathbf{f}.$$

Here $\tilde{\mathbf{f}} = \{\tilde{f}_k\}_{k=-\frac{N}{2}}^{\frac{N}{2}-1} \in \mathbb{C}^N$, and $\mathbf{F} \in \mathbb{C}^{N \times N}$ is the discrete Fourier transform (DFT) matrix with entries

$$\mathbf{F}(n, j) = \frac{1}{N} e^{-i(n-\frac{N}{2}-1)\pi x_j}, \quad 1 \leq n, j \leq N.$$

Analogously, given Fourier coefficients $\hat{\mathbf{f}} = \{\hat{f}_k\}_{k=-\frac{N}{2}}^{\frac{N}{2}-1} \in \mathbb{C}^N$ in (2.2), we write the corresponding discrete Fourier partial sum for (2.3) as

$$(3.3) \quad \mathbf{f}_N = \hat{\mathbf{F}}^* \hat{\mathbf{f}},$$

where $\hat{\mathbf{F}}^* \in \mathbb{C}^{N \times N}$ is the (un-normalized) complex conjugate transpose of \mathbf{F} in (3.2), also referred to as the discrete inverse Fourier transform operator with entries³

$$\hat{\mathbf{F}}^*(j, n) = e^{i(n-\frac{N}{2}-1)\pi x_j}, \quad 1 \leq j, n \leq N.$$

Observe that $\mathbf{f}_N = \{S_N f(x_j)\}_{j=1}^N \in \mathbb{R}^N$ due to cancellation of the imaginary terms.

Remark 3.1. *Due to aliasing, (3.2) is not equivalent to (2.2), with the explicit relationship given by (see e.g. [28])*

$$\tilde{f}_k = \hat{f}_k + \sum_{\substack{|q| \leq \infty \\ q \neq 0}} \hat{f}_{k+\frac{Nq}{2}}, \quad -\frac{N}{2} \leq k \leq \frac{N}{2} - 1,$$

which we will write simply as

$$(3.4) \quad \hat{\mathbf{f}} = \tilde{\mathbf{f}} + \boldsymbol{\delta}_f = \mathbf{F}\mathbf{f} + \boldsymbol{\delta}_f,$$

with $\boldsymbol{\delta}_f \in \mathbb{C}^N$ representing the aliasing error. It is typically assumed that the magnitude components of $\boldsymbol{\delta}_f$ are smaller than those in $\hat{\boldsymbol{\epsilon}} = \{\epsilon_k\}_{k=-\frac{N}{2}}^{\frac{N}{2}-1}$ defined in (2.1), and therefore the model discrepancy is reasonable (see e.g. [6]). Indeed, the traditional observation data model corresponding to (2.1) follows (3.4) and is defined as

$$(3.5) \quad \hat{\mathbf{b}} = \mathbf{F}\mathbf{f} + \tilde{\boldsymbol{\epsilon}},$$

where by construction $\tilde{\boldsymbol{\epsilon}} = \hat{\boldsymbol{\epsilon}} + \boldsymbol{\delta}_f \in \mathbb{C}^N$ follows a circularly-symmetric complex normal distribution. We will use (3.5) in Section 5 and further characterize the noise distribution there.

Remark 3.2. *For simplicity we also use the same notation in (3.3) for the discretized Fourier partial sum given noisy Fourier coefficients $\hat{\mathbf{b}} = \{\hat{b}_k\}_{k=-\frac{N}{2}}^{\frac{N}{2}-1} \in \mathbb{C}^N$ in (2.1). That is, we write*

$$(3.6) \quad \mathbf{f}_N = \hat{\mathbf{F}}^* \hat{\mathbf{b}}.$$

Which of (3.3) or (3.6) is employed will be contextually evident.

³The basis $\{e^{ik\pi x}\}_{k \in \mathbb{Z}}$ is orthogonal but not normalized, and there are different conventions for defining the discrete Fourier and inverse Fourier transform to account for the normalizing term (see e.g. [28]). With a slight abuse of notation, we adopt the definitions of \mathbf{F} and $\hat{\mathbf{F}}^*$ in (3.2) and (3.3) which are consistent with our numerical implementation.

The corresponding discrete Gegenbauer partial sum (2.12) can be written as

$$(3.7) \quad \mathbf{f}_m^\lambda = \mathbf{F}^{Geg} \widehat{\mathbf{f}}^\lambda,$$

where $\mathbf{f}_m^\lambda = \{P_m^\lambda f(x_j)\}_{j=1}^N \in \mathbb{R}^N$ and $\widehat{\mathbf{f}}^\lambda = \{\widehat{f}_l^\lambda\}_{l=0}^m \in \mathbb{R}^{m+1}$. Here $\mathbf{F}^{Geg} \in \mathbb{R}^{N \times (m+1)}$ with entries

$$(3.8) \quad \mathbf{F}^{Geg}(j, n) = C_{n-1}^\lambda(x_j), \quad 1 \leq j \leq N, \quad 1 \leq n \leq m+1.$$

Since the Gegenbauer coefficients $\widehat{\mathbf{f}}^\lambda$ in (2.13) are not explicitly known for our problem, we use the composite trapezoidal rule to obtain the approximation

$$(3.9) \quad \widetilde{f}_l^\lambda = \frac{1}{h_l^\lambda} \cdot \frac{2}{N} \sum_{j=1}^N (1-x_j^2)^{\lambda-\frac{1}{2}} f(x_j) C_l^\lambda(x_j), \quad l = 0, \dots, m,$$

as the components of $\widetilde{\mathbf{f}}^\lambda \in \mathbb{R}^{m+1}$, noting that the integrand evaluation vanishes at both boundaries for $\lambda > \frac{1}{2}$ and that the smoothness of the integrand increases with λ . Combining (3.8) and (3.9) yields

$$(3.10) \quad \widetilde{\mathbf{f}}^\lambda = \mathbf{F}^{CT} \mathbf{f}, \quad \mathbf{F}^{CT} = \frac{2}{N} \mathbf{H} \left(\mathbf{F}^{Geg} \right)^T \mathbf{W}.$$

Here $\mathbf{H} \in \mathbb{R}^{(m+1) \times (m+1)}$ is the diagonal normalizing matrix with entries $\mathbf{H}(l, l) = \frac{1}{h_l^\lambda}$ and $\mathbf{W} \in \mathbb{R}^{N \times N}$ is the diagonal weighting matrix with entries $\mathbf{W}(j, j) = (1-x_j^2)^{\lambda-\frac{1}{2}}$.

Related to the discussion in Remark 3.1, there is a quadrature error associated with the Gegenbauer coefficients which we simply write as

$$(3.11) \quad \widehat{\mathbf{f}}^\lambda = \widetilde{\mathbf{f}}^\lambda + \boldsymbol{\delta}_g = \mathbf{F}^{CT} \mathbf{f} + \boldsymbol{\delta}_g,$$

so that the corresponding model for (3.7) is

$$(3.12) \quad \mathbf{f}_m^\lambda = \mathbf{F}^{Geg} \widetilde{\mathbf{f}}^\lambda + \mathbf{F}^{Geg} \boldsymbol{\delta}_g = \mathbf{F}^{Geg} \mathbf{F}^{CT} \mathbf{f} + \widetilde{\boldsymbol{\delta}}_g,$$

where $\widetilde{\boldsymbol{\delta}}_g = \mathbf{F}^{Geg} \boldsymbol{\delta}_g$ can be considered as noise resulting from not having the exact Gegenbauer coefficients $\widehat{\mathbf{f}}^\lambda$. Moreover, assuming large enough N , the error $\boldsymbol{\delta}_g$ incurred using (3.9) is typically smaller than the overall error in the approximation due to the additive noise in (2.1).

Finally, we provide the discretized model for spectral reprojection in (2.21). This is accomplished by first defining $\widehat{\mathbf{g}}^\lambda = \{\widehat{g}_l^\lambda\}_{l=0}^m$, with each component \widehat{g}_l^λ given by (2.20), which we write as

$$(3.13) \quad \widehat{\mathbf{g}}^\lambda = \mathbf{F}^{Bessel} \widehat{\mathbf{b}}.$$

Here $\mathbf{F}^{Bessel} \in \mathbb{C}^{(m+1) \times N}$ has entries

$$(3.14) \quad \mathbf{F}^{Bessel}(j, n) = \begin{cases} 1 & \text{if } j = 1 \text{ and } n = \frac{N}{2} + 1, \\ 0 & \text{if } j > 1 \text{ and } n = \frac{N}{2} + 1, \\ \Gamma(\lambda) i^{j-1} (j-1+\lambda) J_{j-1+\lambda}(\pi k) \left(\frac{2}{\pi k} \right)^\lambda & \text{otherwise,} \end{cases}$$

for $1 \leq j \leq m+1$, $1 \leq n \leq N$ and $k = n - \frac{N}{2} - 1$.

By defining $\mathbf{f}_{m,N}^\lambda = \{f_{m,N}^\lambda(x_j)\}_{j=1}^N$, we have the discretized formulation of (2.21):

$$(3.15) \quad \mathbf{f}_{m,N}^\lambda = \mathbf{F}^{Geg} \widehat{\mathbf{g}}^\lambda = \mathbf{F}^{Geg} \mathbf{F}^{Bessel} \widehat{\mathbf{b}}.$$

Note that (3.15) is *directly* obtained from the given measurements $\widehat{\mathbf{b}}$ in (2.1), that is, there is no additional model error (noise) incurred by implementation. Therefore, when comparing (3.15) to (3.12), we obtain the observation model

$$(3.16) \quad \mathbf{f}_{m,N}^\lambda = \mathbf{f}_m^\lambda + \boldsymbol{\epsilon}^\lambda = \mathbf{F}^{Geg} \mathbf{F}^{CT} \mathbf{f} + \boldsymbol{\epsilon}^\lambda,$$

where the additive noise $\boldsymbol{\epsilon}^\lambda$ has contributions both from $\widehat{\boldsymbol{\epsilon}}$ in (2.1) and $\widetilde{\boldsymbol{\delta}}_g$ in (3.12).

4. A Bayesian framework for spectral reprojection. Spectral reprojection has been successfully used to recover non-periodic (or piecewise smooth) functions from Fourier data in a variety of contexts, including post-processing solutions for numerical conservation laws [28] and recovering images for segmentation purposes [3]. Although some noise is always present, either in the form of numerical simulation error or data acquisition error, most studies have not formally analyzed its contribution to the overall error. However, in [5] it was shown that while the Gegenbauer approximation is an unbiased estimator for additive Gaussian noise, the variance depends on the particular approximation location, with increased variance near the boundaries (or edge locations of piecewise smooth functions). Filtering can reduce the overall variance, but requires further tuning, and moreover leads to a loss of resolution. These issues motivate us to gain a better understanding of the spectral reprojection method using a statistical framework, as we now describe.

We first note that the proof of Theorem 2.1, and specifically the triangular inequality (2.17), provides a blueprint for formulating a Bayesian approach. In particular the inequality also holds for $\|\cdot\|_2$ up to a constant.⁴ Second, the data error term E_D in (2.17) is analogous to the likelihood term in a *maximum a posteriori* (MAP) estimate for a posterior distribution of the unknown signal \mathbf{f} in the discretized framework. Finally, the regularization error term E_R in (2.17) measures the difference between the function and its Gegenbauer partial sum approximation (2.12), which can be viewed as our prior belief about \mathbf{f} . That is, we expect the signal \mathbf{f} to be close to \mathbf{f}_m^λ in (3.12). In a nutshell, these insights allow us to view spectral reprojection from a Bayesian perspective for fixed values of m and λ . We will refer to this approach as the *Bayesian Spectral Reprojection (BSR)* method.

Remark 4.1. As our numerical experiments will show in Section 6, the Bayesian spectral reprojection method yields estimates that are similar to those determined from Algorithm 2.1, which is to be expected based on its design. An advantage to our new Bayesian formulation is that unlike other traditionally chosen priors (e.g. sparse priors), its derivation is motivated by rigorous error approximation analysis. Moreover, as we will describe below, it is also possible to partially quantify the uncertainty of the underlying approximation.

4.1. Statistical formulation for spectral reprojection. Inspired by the spectral reprojection method as discretized by (3.12) and (3.15), we now seek a statistical formulation for the recovery of the unknown signal \mathbf{f} . We begin by considering the linear inverse problem

$$(4.1) \quad \mathcal{G} = \mathcal{A}\mathcal{X} + \mathcal{E},$$

where \mathcal{X} , \mathcal{G} , and \mathcal{E} are random variables defined over a common probability space, and \mathcal{X} and \mathcal{E} are assumed to be independent. In this framework \mathcal{X} represents the unknown which we seek to recover, \mathcal{G}

⁴Using $\|\cdot\|_2$ is convenient because it provides easier analysis and implementation for the corresponding inverse problem. The Bayesian approach can also be used for other norms.

denotes the observables, \mathcal{A} is a known linear operator, and $\mathcal{E} \sim \mathcal{N}(\mathbf{0}, \gamma^{-1}\mathbf{I}_N)$ is a vector of independent and identically distributed (i.i.d.) Gaussian noise with mean 0 and unknown variance γ^{-1} . Finally throughout this manuscript we use \mathbf{I}_N to denote the $N \times N$ identity matrix.

Remark 4.1. *As already noted, the variance of the Gegenbauer approximation has non-trivial expression and depends on the particular approximation location [5]. The assumption about the covariance matrix of \mathcal{E} being a constant multiple of the identity matrix therefore generally does not hold. We nevertheless adopt it for simplicity in (4.1).*

With (3.16) representing the observational model system, the realizations of each random variable in (4.1) respectively are the unknown vector of interest $\mathbf{f} \in \mathbb{R}^N$, the observable data $\mathbf{f}_{m,N}^\lambda \in \mathbb{R}^N$ in (3.15), and noise vector $\boldsymbol{\epsilon}^\lambda \in \mathbb{R}^N$. A hierarchical Bayesian model based on Bayes' theorem then provides an estimate of the full *posterior* distribution given by

$$(4.2) \quad p_{\mathcal{X},\Theta|\mathcal{G}}(\mathbf{f}, \boldsymbol{\theta} | \mathbf{f}_{m,N}^\lambda) \propto p_{\mathcal{G}|\mathcal{X},\Theta}(\mathbf{f}_{m,N}^\lambda | \mathbf{f}, \boldsymbol{\theta}) p_{\mathcal{X}|\Theta}(\mathbf{f} | \boldsymbol{\theta}) p_{\Theta}(\boldsymbol{\theta}),$$

where $p_{\mathcal{G}|\mathcal{X},\Theta}(\mathbf{f}_{m,N}^\lambda | \mathbf{f}, \boldsymbol{\theta})$ is the likelihood density function determined by relationship between \mathbf{f} and $\mathbf{f}_{m,N}^\lambda$ and assumptions on \mathcal{E} , $p_{\mathcal{X}|\Theta}(\mathbf{f} | \boldsymbol{\theta})$ is the density of the prior distribution encoding *a priori* assumptions about the solution, and $p_{\Theta}(\boldsymbol{\theta})$ is the hyperprior density for all other involved parameters, which we denote collectively as $\boldsymbol{\theta}$. In our investigation $p_{\Theta}(\boldsymbol{\theta}) = p_\gamma(\gamma) p_\beta(\beta)$, where γ, β corresponds to the inverse noise and inverse prior variances respectively (see Section 4.4). Note that the right hand side of (4.2) is not normalized (hence \propto is used), but as the normalized version is often not computationally tractable, it is the posterior typically sought in Bayesian inference methods. In what follows we describe how to construct the corresponding likelihood, prior and hyperprior density functions.

4.2. Formulating the likelihood. The likelihood density function $p(\mathbf{f}_{m,N}^\lambda | \mathbf{f}, \gamma)$ in (4.2) models the connection between the signal and observation vectors.⁵ expressions for each density function in (4.2). As already noted, the data error term E_D in (2.17) states intuitively that $\mathbf{f}_{m,N}^\lambda$ is close to \mathbf{f}_m^λ , while \mathbf{f}_m^λ is related to the underlying signal \mathbf{f} via (3.12). This insight allows us to define the observation model as (3.16), and more specifically to prescribe the distribution for the likelihood as

$$(4.3) \quad \mathbf{f}_{m,N}^\lambda \sim \mathcal{N}(\mathbf{F}^{Geg} \mathbf{F}^{CT} \mathbf{f}, \gamma^{-1} \mathbf{I}),$$

with the interpretation that the data error $\boldsymbol{\epsilon}^\lambda = \mathbf{f}_{m,N}^\lambda - \mathbf{F}^{Geg} \mathbf{F}^{CT} \mathbf{f}$ corresponding to E_D follows the distribution $\mathcal{N}(\mathbf{0}, \gamma^{-1} \mathbf{I}_N)$ for unknown variance γ^{-1} . Thus

$$(4.4) \quad p(\boldsymbol{\epsilon}^\lambda | \gamma) = \left(\frac{\gamma}{2\pi} \right)^{\frac{N}{2}} \exp \left(-\frac{\gamma}{2} \|\boldsymbol{\epsilon}^\lambda\|_2^2 \right).$$

The likelihood density function is determined entirely from (4.4), yielding

$$(4.5) \quad p(\mathbf{f}_{m,N}^\lambda | \mathbf{f}, \gamma) = \left(\frac{\gamma}{2\pi} \right)^{\frac{N}{2}} \exp \left(-\frac{\gamma}{2} \|\mathbf{f}_{m,N}^\lambda - \mathbf{F}^{Geg} \mathbf{F}^{CT} \mathbf{f}\|_2^2 \right).$$

Importantly, we observe that $\mathbf{f}_{m,N}^\lambda = \mathbf{F}^{Geg} \mathbf{F}^{Bessel} \widehat{\mathbf{b}}$ is obtained *directly* by linear transformation of the measurement data $\widehat{\mathbf{b}}$ via (3.15).

⁵To avoid cumbersome notation, henceforth we adopt simplified

4.3. Formulating the prior. The prior function models our prior belief about the unknown signal \mathbf{f} . In this investigation $\mathbf{f} = \{f(x_j)\}_{j=1}^N$ where f is analytic in $[-1, 1]$, and hence, due to (2.8), a distribution for the true solution \mathbf{f} can be motivated using (3.12), resulting in

$$(4.6) \quad \mathcal{X} \sim \mathcal{N}(\mathbf{f}_m^\lambda, \beta^{-1} \mathbf{I}_N),$$

where \mathbf{f}_m^λ is the Gegenbauer partial sum approximation in (3.12) with a hyperprior $\beta > 0$ being inverse variance. Essentially, since the regularization error term E_R measures the difference between the function and its approximation with Gegenbauer basis, we expect the signal \mathbf{f} to be close to \mathbf{f}_m^λ , leading to the conditionally Gaussian prior function

$$(4.7) \quad p(\mathbf{f} | \beta) = \left(\frac{\beta}{2\pi}\right)^{\frac{N}{2}} \exp\left(-\frac{\beta}{2} \|(\mathbf{I}_N - \mathbf{F}^{Geg} \mathbf{F}^{CT}) \mathbf{f}\|_2^2\right).$$

A few remarks are in order:

Remark 4.2 (Choice of λ). *Our choice for λ is motivated by Theorem 2.1, even though our underlying assumption about f being analytic in $[-1, 1]$ means that it can be approximated equally well by any orthogonal polynomial expansion (2.4), that is for all $\lambda \geq 0$. For the trapezoidal rule to be accurate using equally spaced nodes ((3.9) and later (4.7)) a sufficient number of vanishing derivatives of the integrand function at ± 1 is needed, further motivating the use of “large enough” λ . By contrast, it was demonstrated in [11] that if λ is too large, the Gegenbauer reprojection method yields poor results, mainly due to the narrow region of support of $w_\lambda(x)$ (Definition 2.1). To this end we note that other Gibbs complementary bases, such as the Freud polynomials used in [20], are more robust. The benefits in this case are only realized when N is very large, a consequence of the resolution requirements for the corresponding polynomial approximation. As it is important in the context of inverse problems that the solution be obtainable without a large number of measurements, we restrict our study to Gegenbauer polynomials. Our specific choices for λ , especially as a function of signal-to-noise ratio SNR, is discussed in more detail in subsection 6.3.*

Remark 4.3 (Choice of m). *We also choose m to satisfy Theorem 2.1, which follows from (2.8). Although it is possible to make both λ and m unknown random variables, this will greatly increase the computational cost owing to the computation of \mathbf{F}^{Geg} and \mathbf{F}^{CT} which would no longer be deterministic. In particular the dimensions of \mathbf{F}^{Geg} would change for each iteration. Since our prior pertains to the analyticity of the underlying function f , adopting m according to (2.8) is reasonable.*

Remark 4.4 (Sparse priors). *Priors are often constructed to satisfy the assumption that the underlying solution is sparse in some transform domain, such as the gradient or wavelet domain, see e.g. [15, 22, 27, 30] and references therein. From this perspective, since the decay of the orthogonal polynomial coefficients for f is exponential, we could construct a sparse prior where the transform domain is computed in (3.10) for $\lambda \geq 0$. The resulting prior would be similar to those used in the above references with the notable exception that for $m \sim \kappa N$ satisfying Theorem 2.1, we are allowing the underlying function to have considerable variability, which is much less restrictive than using the gradient or low-order wavelet transforms. Since our goal is to express spectral reprojection in a Bayesian framework, we do not compare our new method to formulations using sparse priors in this investigation.*

4.4. Formulating the hyperpriors. In (4.2) we denoted $p(\boldsymbol{\theta})$ as the hyperprior density function for any additional parameters needed to describe the hierarchical model. As noted there, this amounts to $p(\boldsymbol{\theta}) = p(\gamma) p(\beta)$, with γ, β being the inverse noise variance and inverse prior variance respectively. Choosing γ and β to be Gamma distributions is convenient since their corresponding densities are conjugate for the corresponding conditionally Gaussian distributions (4.5) and (4.7).

The Gamma distribution has probability density function

$$(4.8) \quad \Gamma(\eta | c, d) = \frac{d^c}{\Gamma(c)} \eta^{c-1} e^{-d\eta},$$

where c and d are positive shape and rate parameters. For $c \rightarrow 1$ and $d \rightarrow 0$, (4.8) is an uninformative prior, which is desirable since we do not want these parameters to have undue influence on the solution. Thus here for simplicity we choose

$$(4.9a) \quad p(\gamma) = \Gamma(\gamma | c, d),$$

$$(4.9b) \quad p(\beta) = \Gamma(\beta | c, d).$$

with $c = 1$ and $d = 10^{-4}$ for all of our numerical examples.⁶ Following the above discussion, we then replace $p(\boldsymbol{\theta})$ in (4.2) with

$$(4.10) \quad p(\boldsymbol{\theta}) = p(\gamma)p(\beta) \propto \gamma^{c-1} \exp(-d\gamma) \beta^{c-1} \exp(-d\beta).$$

4.5. Bayesian inference. We now have all of the ingredients needed to construct (4.2). Specifically, substituting in the likelihood (4.5), the prior (4.7) and the hyperprior (4.10) density functions into (4.2), we obtain the posterior density function approximation

$$(4.11) \quad p(\mathbf{f}, \gamma, \beta | \mathbf{f}_{m,N}^\lambda) \propto \gamma^{c+\frac{N}{2}-1} \beta^{c+\frac{N}{2}-1} \exp \left\{ -\frac{\gamma}{2} \|\mathbf{f}_{m,N}^\lambda - \mathbf{F}^{Geg} \mathbf{F}^{CT} \mathbf{f}\|_2^2 - \frac{\beta}{2} \|(\mathbf{I}_N - \mathbf{F}^{Geg} \mathbf{F}^{CT}) \mathbf{f}\|_2^2 - d\gamma - d\beta \right\}.$$

From here we can obtain the MAP estimate, which is equivalent to minimizing the negative logarithm of the right hand side of (4.11), yielding the objective function

$$(4.12) \quad \begin{aligned} \mathcal{J}(\mathbf{f}, \gamma, \beta) &= -(c + \frac{N}{2} - 1) \log(\gamma) - (c + \frac{N}{2} - 1) \log(\beta) + \frac{\gamma}{2} \|\mathbf{f}_{m,N}^\lambda - \mathbf{F}^{Geg} \mathbf{F}^{CT} \mathbf{f}\|_2^2 \\ &+ \frac{\beta}{2} \|(\mathbf{I}_N - \mathbf{F}^{Geg} \mathbf{F}^{CT}) \mathbf{f}\|_2^2 + d\gamma + d\beta \end{aligned}$$

up to a constant that is independent of \mathbf{f} , γ , and β . In what follows we discuss how to minimize (4.12).

4.5.1. The block-coordinate descent approach. We use a block-coordinate descent (BCD) approach [43, 8] to approximate the MAP estimate of (4.11). In particular, BCD minimizes \mathcal{J} in (4.12) by alternating minimization w.r.t. \mathbf{f} for fixed γ, β , minimization w.r.t. γ for fixed \mathbf{f}, β , and minimization w.r.t. β for fixed \mathbf{f}, γ . That is, given an initial guess for the hyperparameters γ and β , the BCD algorithm proceeds through a sequence of updates of the form

$$(4.13a) \quad \mathbf{f} = \arg \min_{\mathbf{f}} \{ \mathcal{J}(\mathbf{f}, \gamma, \beta) \},$$

$$(4.13b) \quad \gamma = \arg \min_{\gamma} \{ \mathcal{J}(\mathbf{f}, \gamma, \beta) \},$$

$$(4.13c) \quad \beta = \arg \min_{\beta} \{ \mathcal{J}(\mathbf{f}, \gamma, \beta) \},$$

until a convergence criterion is met. In our implementation we initialize the hyperparameter vectors as $\gamma = 1$ and $\beta = 1$, and we stop when either the relative change of the objective function value or the relative change in \mathbf{f} falls below a given threshold. Efficient implementation of the three update steps in (4.13) is described below.

⁶For more detailed explanations regarding this choice of hyperprior, see [15, 22] and references therein.

4.5.2. Updating the unknown signal \mathbf{f} . Due to our intentionally chosen conditionally Gaussian prior (4.7) and Gamma hyperprior (4.9a) – (4.9b), for fixed γ and β we have

$$(4.14) \quad p(\mathbf{f}, \gamma, \beta | \mathbf{f}_{m,N}^\lambda) \propto p(\mathbf{f}_{m,N}^\lambda | \mathbf{f}, \gamma) p(\mathbf{f} | \beta) \propto \mathcal{N}(\boldsymbol{\mu}, C),$$

where

$$(4.15) \quad \boldsymbol{\mu} = \gamma C (\mathbf{F}^{Geg} \mathbf{F}^{CT})^T \mathbf{f}_{m,N}^\lambda$$

and

$$(4.16) \quad C = \left(\gamma (\mathbf{F}^{Geg} \mathbf{F}^{CT})^T (\mathbf{F}^{Geg} \mathbf{F}^{CT}) + \beta (\mathbf{I}_N - \mathbf{F}^{Geg} \mathbf{F}^{CT})^T (\mathbf{I}_N - \mathbf{F}^{Geg} \mathbf{F}^{CT}) \right)^{-1}.$$

The update step for \mathbf{f} in (4.13a) therefore reduces to solving the linear system

$$(4.17) \quad \left(\gamma (\mathbf{F}^{Geg} \mathbf{F}^{CT})^T (\mathbf{F}^{Geg} \mathbf{F}^{CT}) + \beta (\mathbf{I}_N - \mathbf{F}^{Geg} \mathbf{F}^{CT})^T (\mathbf{I}_N - \mathbf{F}^{Geg} \mathbf{F}^{CT}) \right) \mathbf{f} = \gamma (\mathbf{F}^{Geg} \mathbf{F}^{CT})^T \mathbf{f}_{m,N}^\lambda.$$

We also note that by construction the *common kernel condition* (see e.g. [31])

$$(4.18) \quad \text{kernel}(\mathbf{F}^{Geg} \mathbf{F}^{CT}) \cap \text{kernel}(\mathbf{I}_N - \mathbf{F}^{Geg} \mathbf{F}^{CT}) = \{\mathbf{0}\}$$

is automatically satisfied, and hence (4.17) has a unique solution which can be directly obtained.

Remark 4.5. Recall that the kernel of an operator $G : \mathbb{C}^N \rightarrow \mathbb{C}^M$ is given by $\text{kernel}(G) = \{\mathbf{f} \in \mathbb{C}^N \mid G\mathbf{f} = \mathbf{0}\}$, that is, the set of vectors that are mapped to zero. The common kernel condition (4.18) ensures that the prior (regularization) introduces a sufficient amount of complementary information to the likelihood (the given measurements) to make the problem well-posed, which is a standard assumption in regularized inverse problems [31, 40].

Analogous to the objective function (4.12), we also note that (4.17) is equivalent to updating \mathbf{f} via the quadratic optimization problem

$$(4.19) \quad \mathbf{f} = \arg \min_{\mathbf{f}} \left\{ \frac{\gamma}{2} \|\mathbf{f}_{m,N}^\lambda - \mathbf{F}^{Geg} \mathbf{F}^{CT} \mathbf{f}\|_2^2 + \frac{\beta}{2} \|(\mathbf{I}_N - \mathbf{F}^{Geg} \mathbf{F}^{CT}) \mathbf{f}\|_2^2 \right\}.$$

Various methods can be used to efficiently solve (4.19), including the fast iterative shrinkage-thresholding (FISTA) algorithm [9], the preconditioned conjugate gradient (PCG) method [36], potentially combined with an early stopping based on Morozov’s discrepancy principle [12, 13, 14], and the gradient descent approach [22]. There is no general advantage of one method over another, and the choice should be made based on the specific problem at hand.

4.5.3. Updating the hyperparameters γ and β . We now address the update for the hyperparameter γ for fixed \mathbf{f} and β . Substituting (4.12) into (4.13b) and ignoring all terms that do not depend on γ yields

$$(4.20) \quad \gamma = \arg \min_{\gamma} \{ \mathcal{J}_\gamma \} = \arg \min_{\gamma} \left\{ -\left(c + \frac{N}{2} - 1\right) \log(\gamma) + \frac{\gamma}{2} \|\mathbf{f}_{m,N}^\lambda - \mathbf{F}^{Geg} \mathbf{F}^{CT} \mathbf{f}\|_2^2 + d\gamma \right\}.$$

Solving $\frac{d\mathcal{J}_\gamma}{d\gamma} = 0$ then provides

$$(4.21) \quad \gamma = \frac{2c + N - 2}{\|\mathbf{f}_{m,N}^\lambda - \mathbf{F}^{Geg} \mathbf{F}^{CT} \mathbf{f}\|_2^2 + 2d}$$

for the γ -update. The β -update is similarly obtained as

$$(4.22) \quad \beta = \frac{2c + N - 2}{\|(\mathbf{I}_N - \mathbf{F}^{Geg} \mathbf{F}^{CT}) \mathbf{f}\|_2^2 + 2d}.$$

Algorithm 4.1 summarizes the iterative process for finding the point estimate solution \mathbf{f} in (4.13) along with precision values γ and β .

Algorithm 4.1 The Bayesian spectral reprojection (BSR) MAP estimate

Input Data vector $\hat{\mathbf{b}} \in \mathbb{C}^N$ in (2.1), choices for $\lambda = \kappa_1 N$ and $m = \kappa_2 N$, $0 < \kappa_1, \kappa_2 < 1$, and grid points x_j , $j = 1, \dots, N$.

Output MAP estimates for \mathbf{f} , γ , and β .

Initialize γ and β . We choose $\gamma = \beta = 1$.

Calculate the likelihood $\mathbf{f}_{m,N}^\lambda$ according to (3.15).

repeat

 Update \mathbf{f} according to (4.17)

 Update γ according to (4.21)

 Update β according to (4.22)

until convergence or the maximum number of iterations is reached

Remark 4.2 (Fixed hyperparameters). We note that the posterior formulation in (4.11) allows for uncertainty quantification for the recovered solution \mathbf{f} for *fixed* γ and β . Specifically, from (4.14) we have

$$(4.23) \quad p(\mathbf{f} | \mathbf{f}_{m,N}^\lambda) \propto p(\mathbf{f}_{m,N}^\lambda | \mathbf{f}) p(\mathbf{f}) \propto \mathcal{N}(\boldsymbol{\mu}, C),$$

where the mean $\boldsymbol{\mu}$ and the covariance matrix C are again respectively given by (4.15) and (4.16). We can then sample directly from $\mathcal{N}(\boldsymbol{\mu}, C)$ to obtain credible intervals⁷ for every component of the solution \mathbf{f} . When γ and β are themselves random variables, computational sampling is needed to recover (4.11), for instance, full posterior sampling using a Markov chain Monte Carlo (MCMC) method [34], typically requiring considerable computational expense.

5. Generalized Bayesian spectral reprojection. By design, and as will be demonstrated via numerical experiments in Section 6, the BSR method in Algorithm 4.1 yields comparable point estimates as the original spectral reprojection method in Algorithm 2.1. We are furthermore able to quantify the uncertainty of the approximation for fixed hyperparameters γ and β (see Remark 4.2). Several potential shortcomings of the BSR approach are readily apparent, however. Specifically, methods for computational inverse problems are designed to promote solutions that yield close approximations to the observable information while also being constrained by assumptions regarding the underlying signal. In addition to mitigating the effects of ill-posedness, the regularization (prior) term also serves to avoid over-fitting. By construction, the likelihood and prior terms in posterior density function (4.11) are *both* based on the assumption that $f \in \mathbb{P}_m^\lambda$, that is, the space of Gegenbauer polynomials given by (2.4). While such an assumption is suitable for solving the *forward* problem in Algorithm 2.1, it inherently limits the space of possible solutions when considering the *inverse* problem. A more natural approach for solving linear inverse problems with i.i.d. additive (complex) Gaussian noise is to *directly* fit the given

⁷Related to the (frequentist) confidence interval, a (Bayesian) credible interval is used to characterize a probability distribution, and is also sometimes referred to as a Bayesian posterior interval [32, 21].

data model in the construction of the likelihood, and then determine a suitable prior (regularization) for fitting the data model. In this regard, our insights in using the spectral projection prior (4.7) still remain, in particular pertaining to the discussion in Remark 4.2 and Remark 4.3.

Given these insights, we now introduce the *generalized* Bayesian spectral projection (GBSR) method. We demonstrate its advantages in generating the MAP estimate with regard to accuracy and robustness in our numerical experiments in section 6, where we also display credible intervals for fixed hyperparameters.

5.1. Formulating the inverse problem. We begin by considering the linear inverse problem

$$(5.1) \quad \widehat{\mathcal{B}} = \mathcal{F}\mathcal{X} + \widetilde{\mathcal{E}},$$

where \mathcal{X} , $\widehat{\mathcal{B}}$, and $\widetilde{\mathcal{E}}$ are random variables defined over a common probability space, and \mathcal{X} and $\widetilde{\mathcal{E}}$ are assumed to be independent. As before, \mathcal{X} represents the unknown which we seek to recover, $\widehat{\mathcal{B}}$ denotes the observables, \mathcal{F} is a known linear operator, and $\widetilde{\mathcal{E}} \sim \mathcal{CN}(\mathbf{0}, \widetilde{\gamma}^{-1}\mathbf{I}_N)$ is a vector of independent and identically distributed (i.i.d.) circularly symmetric complex Gaussian noise with mean 0 and unknown variance $\widetilde{\gamma}^{-1}$.⁸ The realizations of the random variables in (5.1) are modeled in (3.5), respectively by $\mathbf{f} \in \mathbb{R}^N$, $\widehat{\mathbf{b}} \in \mathbb{C}^N$, and $\widetilde{\boldsymbol{\epsilon}} \in \mathbb{C}^N$.

We now proceed to formulate the corresponding posterior density function given by

$$(5.2) \quad p(\mathbf{f}, \boldsymbol{\theta} | \widehat{\mathbf{b}}) \propto p(\widehat{\mathbf{b}} | \mathbf{f}, \boldsymbol{\theta}) p(\mathbf{f} | \boldsymbol{\theta}) p(\boldsymbol{\theta}),$$

where, analogously to (4.2), $p(\widehat{\mathbf{b}} | \mathbf{f}, \boldsymbol{\theta})$ is the likelihood density function determined by \mathbf{F} in (3.5) and assumptions on $\widetilde{\mathcal{E}}$, $p(\mathbf{f} | \boldsymbol{\theta})$ is the density of the prior distribution encoding *a priori* assumptions about the solution, and $p(\boldsymbol{\theta})$ is the hyperprior density for all other involved parameters, which we denote collectively as $\boldsymbol{\theta}$. As was also done in Section 4, we write $p(\boldsymbol{\theta}) = p(\widetilde{\gamma}) p(\beta)$, where $\widetilde{\gamma}$ and β correspond to the inverse noise and inverse prior variances respectively.

5.2. Formulating the likelihood. Since $\widetilde{\mathcal{E}} \sim \mathcal{CN}(\mathbf{0}, \widetilde{\gamma}^{-1}\mathbf{I}_N)$ for unknown variance $\widetilde{\gamma}^{-1}$, we have

$$p(\widetilde{\boldsymbol{\epsilon}} | \widetilde{\gamma}) = \left(\frac{\widetilde{\gamma}}{\pi}\right)^N \exp\left(-\widetilde{\gamma}\|\widetilde{\boldsymbol{\epsilon}}\|_2^2\right).$$

It follows from (3.5) that the likelihood density function is then

$$(5.3) \quad p(\widehat{\mathbf{b}} | \mathbf{f}, \widetilde{\gamma}) = \left(\frac{\widetilde{\gamma}}{\pi}\right)^N \exp(-\widetilde{\gamma}\|\widehat{\mathbf{b}} - \mathbf{F}\mathbf{f}\|_2^2),$$

with corresponding distribution

$$(5.4) \quad \widehat{\mathcal{B}} \sim \mathcal{CN}(\mathbf{F}\mathbf{f}, \widetilde{\gamma}^{-1}\mathbf{I}_N).$$

5.3. Formulating the prior and the hyperpriors. For reasons already mentioned, we again choose the prior density function to be used in (5.2) as (4.7). We also note that in the context of the likelihood density function given by (5.3), our choice of prior means that the resulting objective function yields enough overlap between the data (likelihood) and regularization (prior) terms to determine a meaningful solution, beyond satisfying the common kernel condition.⁹ Specifically, for $r > 0$ and constants

⁸Unlike the BSR formulation in (4.1), since no transformation is used in (5.1), the noise does truly follow $\mathcal{CN}(\mathbf{0}, \alpha^{-1}\mathbf{I}_N)$ for α^{-1} defined in (2.1), that is, $\widetilde{\gamma} = \alpha$.

⁹Since \mathbf{F} is invertible, $\ker(\mathbf{F}) = \{\mathbf{0}\}$ and the kernel condition for GBSR is automatically satisfied.

$Const_1, C > 0$, (2.8) yields

$$\langle P_m^\lambda f - f, e^{ik\pi x} \rangle \leq Const_1 \int_{-1}^1 e^{-m^r} e^{-ik\pi x} dx < C e^{-rm},$$

and in fact is only nonzero for $k = 0$. Since $m \propto N$, which is assumed to adequately resolve the underlying signal \mathbf{f} from $\widehat{\mathbf{b}}$, we conclude that the solution \mathbf{f} can be recovered for our choice of prior. Furthermore, although only $\lambda \geq 0$ is required to satisfy (2.8), as discussed in Remark 4.2, λ still must be large enough for (3.9) to accurately approximate $\{\widehat{f}_\ell^\lambda\}_{\ell=1}^m$ in (2.7), while small enough to maintain robustness. A complete discussion for choosing in the context of noise is provided in subsection 6.3.

Finally, the hyperpriors $\tilde{\gamma}$ and β are again modeled as Gamma distributions, yielding the hyperprior density function (4.10) density function with $\tilde{\gamma}$ replacing γ as the likelihood hyperprior, i.e.

$$(5.5) \quad p(\boldsymbol{\theta}) = p(\tilde{\gamma})p(\beta) \propto \tilde{\gamma}^{c-1} \exp(-d\tilde{\gamma}) \beta^{c-1} \exp(-d\beta).$$

5.4. Bayesian inference. Substituting the likelihood (5.3), the prior (4.7) and the hyperprior (5.5) density functions into (5.2), we obtain the posterior density function approximation

$$(5.6) \quad p(\mathbf{f}, \tilde{\gamma}, \beta | \widehat{\mathbf{b}}) \propto \tilde{\gamma}^{c+N-1} \beta^{c+\frac{N}{2}-1} \exp \left\{ -\tilde{\gamma} \|\widehat{\mathbf{b}} - \mathbf{F}\mathbf{f}\|_2^2 - \frac{\beta}{2} \|(\mathbf{I}_N - \mathbf{F}^{Geg} \mathbf{F}^{CT})\mathbf{f}\|_2^2 - d\tilde{\gamma} - d\beta \right\}.$$

The MAP estimate of (5.6) is the minimizer of the objective function

$$(5.7)$$

$$\tilde{\mathcal{J}}(\mathbf{f}, \tilde{\gamma}, \beta) = -(c+N-1) \log(\tilde{\gamma}) - (c + \frac{N}{2} - 1) \log(\beta) + \tilde{\gamma} \|\widehat{\mathbf{b}} - \mathbf{F}\mathbf{f}\|_2^2 + \frac{\beta}{2} \|(\mathbf{I}_N - \mathbf{F}^{Geg} \mathbf{F}^{CT})\mathbf{f}\|_2^2 + d\tilde{\gamma} + d\beta$$

up to a constant that is independent of \mathbf{f} , $\tilde{\gamma}$, and β . The BCD algorithm iteratively updates the solution according to

$$(5.8a) \quad \left(2\tilde{\gamma} \mathbf{F}^* \mathbf{F} + \beta (\mathbf{I}_N - \mathbf{F}^{Geg} \mathbf{F}^{CT})^T (\mathbf{I}_N - \mathbf{F}^{Geg} \mathbf{F}^{CT}) \right) \mathbf{f} = 2\tilde{\gamma} \mathbf{F}^* \widehat{\mathbf{b}},$$

$$(5.8b) \quad \tilde{\gamma} = \frac{c+N-1}{\|\widehat{\mathbf{b}} - \mathbf{F}\mathbf{f}\|_2^2 + d},$$

$$(5.8c) \quad \beta = \frac{2c+N-2}{\|(\mathbf{I}_N - \mathbf{F}^{Geg} \mathbf{F}^{CT})\mathbf{f}\|_2^2 + 2d}.$$

Algorithm 5.1 summarizes the iterative process for minimizing the objective function (5.7), which provides the point estimate solution \mathbf{f} along with precision values $\tilde{\gamma}$ and β . Analogous to the formulation obtained in Remark 4.2, for fixed $\tilde{\gamma}$ and β it is possible to directly sample from the resulting posterior to obtain credible intervals.

6. Numerical experiments. We now demonstrate the efficacy of the BSR (Algorithm 4.1) and GSBR (Algorithm 5.1), and compare each method's performance to the original spectral reprojection in Algorithm 2.1. We also test our new methods for varying signal-to-noise ratio (SNR), which we define as

$$(6.1) \quad \text{SNR} = 10 \log_{10} \left(\frac{\|\mathbf{F}\mathbf{f}\|_2^2}{N\alpha^{-1}} \right).$$

In each example the noisy Fourier data $\widehat{\mathbf{b}}$ is given by (2.1) with noise variance α^{-1} corresponding to (6.1). The noiseless N Fourier coefficients $\widehat{\mathbf{f}}$ are constructed via trapezoidal rule (3.1) for a highly resolved mesh ($8N$).

Algorithm 5.1 The Generalized Bayesian spectral reprojection (GBSR) MAP estimate

Input Data vector $\widehat{\mathbf{b}} \in \mathbb{C}^N$ in (2.1), choices for $\lambda = \kappa_1 N$ and $m = \kappa_2 N$, $0 < \kappa_1, \kappa_2 < 1$, and grid points $x_j, j = 1, \dots, N$.

Output MAP estimates for \mathbf{f} , $\tilde{\gamma}$, and β .

Initialize $\tilde{\gamma}$ and β as $\tilde{\gamma} = \beta = 1$.

repeat

 Update \mathbf{f} according to (5.8a)

 Update $\tilde{\gamma}$ according to (5.8b)

 Update β according to (5.8c)

until convergence or the maximum number of iterations is reached

6.1. An illustrative example. We first seek to make a general comparison of the Fourier partial sum approximation given by (3.6), the (Gegenbauer) spectral reprojection in Algorithm 2.1, the BSR approach in Algorithm 4.1, and finally the GBSR method in Algorithm 5.1. We choose an example that is readily recovered for large enough N (number of given Fourier coefficients) in the noise-free case using spectral reprojection for suitable parameter choices m and λ . In particular, we consider the function

$$(6.2) \quad f(x) = e^x \sin(5x), \quad x \in [-1, 1].$$

We assume we are given the first $N = 128$ noisy Fourier samples $\widehat{\mathbf{b}}$ in (2.1) with noise variance $\alpha^{-1} = 2 \times 10^{-3}$ (equivalently $\text{SNR} \approx 5.95$). The spectral reprojection parameters $m = 9$ and $\lambda = 4$ are chosen to satisfy Theorem 2.1 and also to ensure accurate and robust recovery in the noise-free case.

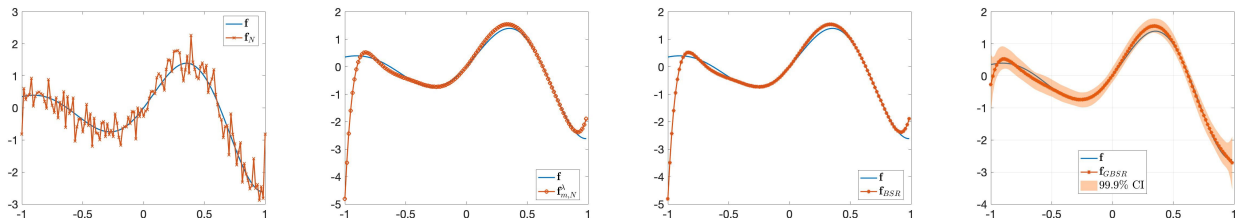


Figure 6.1: Recovery of $f(x) = e^x \sin(5x)$. (left) Fourier reconstruction \mathbf{f}_N in (3.6); (center-left) Spectral reprojection $\mathbf{f}_{m,N}^\lambda$ in Algorithm 2.1; (center-right) \mathbf{f}_{BSR} in Algorithm 4.1; and (right) \mathbf{f}_{GBSR} in Algorithm 5.1.

Figure 6.1 compares the recovery of (6.2) using (3.6), Algorithm 2.1, Algorithm 4.1 and Algorithm 5.1. The 99.9% credible intervals of the solution posterior $p(\mathbf{f} | \widehat{\mathbf{b}})$ using the final (fixed) estimates of the hyperparameters $\tilde{\gamma}$ and β , as described in Remark 4.2, are also displayed. In addition to the Gibbs phenomenon artifacts manifested by the over/undershoots at the boundaries, the Fourier partial sum \mathbf{f}_N clearly yields a noisy approximation. Standard filtering would reduce the oscillations, but also cause excessive blurring [28]. Algorithm 2.1 improves accuracy away from the boundaries, but due to the added noise there are large deviations at the boundaries, especially near $x = -1$. In this regard we note that it was shown in [5] that the variance near the boundaries using the Gegenbauer reconstruction method is *not* reduced when compared to the standard Fourier partial sum. As expected, the point estimate in Algorithm 4.1 yields nearly identical results to those obtained in Algorithm 2.1. The corresponding credible intervals obtained for fixed hyperparameters γ and β (see Remark 4.2) are very

tight and therefore not shown. This is also to be expected following the discussion at the beginning of Section 5, and indeed served to motivate the GBSR approach. Finally, we observe that Algorithm 5.1 yields the overall best results, with better performance throughout the domain. The credible interval is also displayed in Figure 6.1(right).

Remark 6.1. *Due to issues of ill conditioning leading to the Runge phenomenon, the Gegenbauer spectral reconstruction may perform poorly for large λ even though Theorem 2.1 is satisfied [11]. The robust Gibbs complementary (Freud) basis proposed in [20] as the reprojection basis $\{\psi_l^\lambda\}_{l=0}^m$ in (2.4) helps alleviate these issues, but requires more points per wave (large N) to fully resolve the approximation. The approach moreover was considered only for noise-free data. Using the Freud reprojection basis did not yield any noticeable improvement in our experiments. Therefore, given the additional cost incurred in using large N , we do not consider it further.*

6.2. Noise analysis. Now we investigate a more typical scenario in computational inverse problems, that is, with fewer observables and possibly lower SNR. Since it was used in [25], we also consider the non-periodic analytic function $f(x) = \cos(1.4\pi(x + 1))$ on domain $[-1, 1]$. We assume we are given $N = 48$ noisy Fourier coefficients $\hat{\mathbf{b}}$ in (2.1) with different SNR levels, where $\hat{\mathbf{f}}$ are constructed from (3.1) using a refined mesh $8N$.

Remark 6.1 (Noisy versus noise-free data). For the *noiseless* case, it was shown in [25] that choosing $m = \lambda = 9$ yields more accurate results given $N = 48$ Fourier coefficients $\hat{\mathbf{f}}$. However, when the Fourier coefficients contain even small amounts of noise, the performance quality of the spectral reconstruction method rapidly deteriorates. In particular, the ill-conditioning attributed to larger values of λ exacerbates the impact of noise in the approximation. To mitigate these effects, we choose $\lambda = 4$ in our numerical experiments. Note that m , which corresponds to the number of Gegenbauer polynomials needed to resolve the underlying function, is less impacted by noise. Hence $m = 9$ is still appropriate.

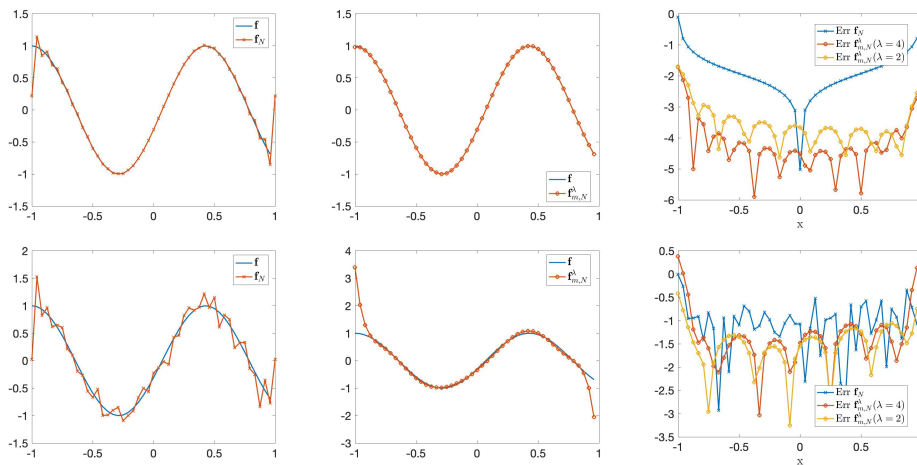


Figure 6.2: (Top-left) Fourier reconstruction \mathbf{f}_N in (3.6); (top-middle) Spectral reconstruction $\mathbf{f}_{m,N}^\lambda$ computed via Algorithm 2.1; (top right) pointwise errors for *noiseless* data for $\lambda = 4$ and $\lambda = 2$. (Bottom) Same experiments with SNR = 10.

To serve as baseline comparisons for the GBSR method, Figure 6.2(top) shows the Fourier partial sum in (3.6) and the Gegenbauer reconstruction obtained from Algorithm 2.1 given noiseless Fourier data. The pointwise errors for $\lambda = 4$ and $\lambda = 2$ are also shown. Clearly, Gegenbauer reconstruction

successfully resolves the Gibbs phenomenon for appropriate choices of λ and m according to [Theorem 2.1](#), with $\lambda = 4$ providing a more accurate approximation than $\lambda = 2$. [Figure 6.2](#)(bottom) shows the same results for SNR = 10. The performance of Gegenbauer reconstruction notably deteriorates, especially near the boundaries, which is attributable to the Runge phenomenon being exacerbated by noise. In this case we observe that $\lambda = 2$ yields better overall performance, and noticeably at the boundaries. [Subsection 6.3](#) provides a more in depth discussion regarding the relationship between SNR and λ .

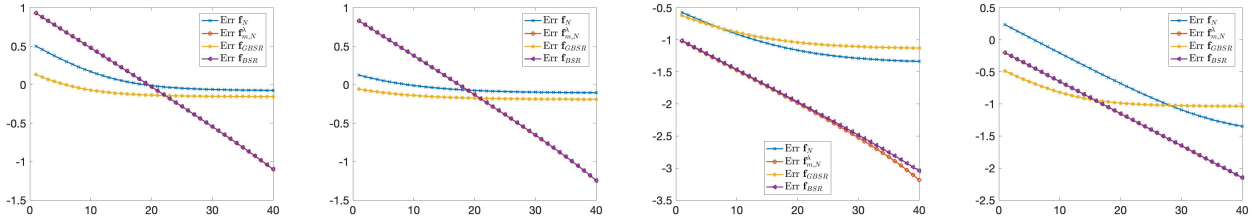


Figure 6.3: Log error plots for varying SNR: (left) l_2 error in $[-1, 1]$, (middle-left) at $x = -1$; (middle-right) at $x = -0.8$; and (right) l_2 error in $[-.5, .5]$ for \mathbf{f}_N , $\mathbf{f}_{m,N}^\lambda$, \mathbf{f}_{BSR} , and \mathbf{f}_{GBSR} .

Figure 6.3 compares errors in logarithmic scale as a function of SNR throughout the interval $[-1, 1]$, at the boundary $x = -1$, at the point $x = -0.8$, and in the interior region from $x = -0.5$ to $x = -0.5$ (chosen to show overall error away from the boundaries). We observe that with increasing SNR, the Gegenbauer approximation $\mathbf{f}_{m,N}^\lambda$ in [Algorithm 2.1](#) starts to converge, as is consistent with [Figure 6.2](#)(right). The point estimate for the BSR method in [Algorithm 4.1](#) is essentially equivalent to the original Gegenbauer reconstruction method. The Fourier partial sum and the GBSR method also produce more accurate approximations with increasing SNR, although as expected each method's convergence rate is not clearly established. The l_2 error in $[-1, 1]$ for all approximations is obviously dominated by the maximum error occurring at $x = -1$. The advantage in using spectral reprojection becomes more apparent away from the boundary, especially with increasing SNR. At $x = -.8$ the GBSR does not yield improvement from standard Fourier reconstruction, even in low SNR environments. By contrast, once we are far enough from the boundary, using [Algorithm 5.1](#) yield more accurate solutions for low SNR. To summarize, in the low SNR regime, the Gegenbauer reconstruction method does not satisfy the conditions for obtaining numerical convergence, especially near the boundary. In this case, the GBSR method provides a relatively reasonable approximation, as well as uncertainty quantification.

6.3. Relationship between SNR and Gegenbauer parameters. [Theorem 2.1](#) establishes the relationship between the number of Fourier coefficients N , the expansion degree in the Gegenbauer polynomial basis m and the corresponding weighting parameter λ . It does not discuss the relationship between these parameters and SNR, however. By design, the BSR method yields MAP estimates that behave similarly to the Gegenbauer reconstruction solution. Specifically, parameters that satisfy [Theorem 2.1](#) yield the best approximations, with $\lambda = \kappa N$ required for small error E_D being analogous to the likelihood term [\(4.3\)](#). On the other hand, $\lambda = \kappa N$ is not required for the GBSR method according to its likelihood distribution [\(5.4\)](#). For *both* methods, when the observables are practically noise-free, there is some non-negligible contribution in using the trapezoidal rule [\(3.1\)](#) for small λ , especially for small N . In all cases, m must be chosen large enough to resolve the underlying function. In this regard, it is important to point out that the parameter m is what describes our *prior* belief. That is, for $m = 0$ we assume the function is constant, for $m = 1$, the function is linear, etc. Indeed, $m = 0$ and $m = 1$ correspond more closely to what is often assumed for image recovery. By contrast, the BSR and GBSR enable the recovery of functions with much greater variability (as dictated by m).

While the choice of m is somewhat independent of SNR, how λ might be chosen changes significantly as SNR decreases. First, any error made using trapezoidal rule is insignificant in low SNR environments. Second, as already discussed, the variance of the Gegenbauer reconstruction method increases at the boundaries. Coupled with the ill-conditioning effects for larger choices of λ , it is not clear how the value of λ affects the performance of each method.

To emphasize the effects of noise on the choice of λ , we consider the same example in [subsection 6.2](#) for varying (integer) values of λ and fixed SNR of 2, 10, and 30. As before we are given $N = 48$ noisy Fourier coefficients $\hat{\mathbf{b}}$ in [\(2.1\)](#) and we again choose $m = 9$ for $\lambda \in [1, 8]$.

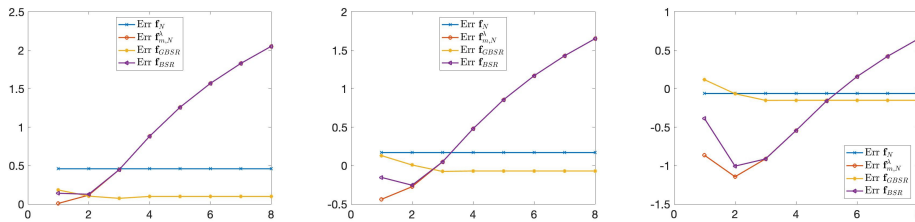


Figure 6.4: Log error plots for varying λ : l_2 error in $[-1, 1]$ with SNR value 2 (left), 10 (middle) and 30 (left) for \mathbf{f}_N , $\mathbf{f}_{m,N}^\lambda$, \mathbf{f}_{BSR} , and \mathbf{f}_{GBSR} .

Figure [6.4](#) compares the l_2 error in $[-1, 1]$ in logarithmic scale with respect to different λ for SNR = 2, 10 and 30. No theoretical justification is available for applying any of these methods in low SNR environments. As SNR increases, it becomes more evident that an optimal λ for both the Gegenbauer reconstruction and BSR methods exists, and is a cumulative result of all the possible considerations already mentioned. On the other hand, the GSB method is clearly robust for various λ values in low SNR environments, mainly because the likelihood term does not involve its use. Of course, none of these methods are a panacea in low SNR environments. The GSB and BSR methods provide additional uncertainty quantification for fixed hyperparameters, although by design the BSR credible interval is quite narrow. We illustrate this in [Figure 6.5](#), where the BSR and GSB approximations are provided along with their respective credible intervals for $\lambda = 2, 4$. Consistent with [Figure 6.4](#), the BSR provides the most accurate results for $\lambda = 2$. The credible interval is very narrow, even in low SNR environments and almost impossible to discern for SNR = 10 and 30. By contrast, we observe nearly identical estimations for $\lambda = 2, 4$ when using GSB. There is furthermore additional information to be gleaned from their credible intervals. Moreover the error near the boundaries appears to be dominated by the likelihood term also having a larger error there, attributable to the over/undershoots caused by the Gibbs phenomenon, as opposed to simply noise (see [Figure 6.2\(left\)](#)).

We emphasize that our numerical experiments are not meant to be prescriptive – that is, it is not the case that one method always outperforms another in all environments. This is to be expected, since [Theorem 2.1](#) has already identified the best solution in the noiseless case. Rather we demonstrate how spectral reprojection inspires two Bayesian approaches, BSR and GSB, both of which can recover analytic non-periodic functions from noisy Fourier data and provide some uncertainty quantification. Indeed, our results suggest that there is justification for choosing a hybrid BSR/GSB approach, one that weighs the BSR more heavily near the boundaries and GSB more heavily in the interior. It is also possible to modify the BSR method so that the likelihood and prior use different parameters for m and λ , which also can be analyzed in the context of the proof of [Theorem 2.1](#). These and other ideas will be explored in future investigations.

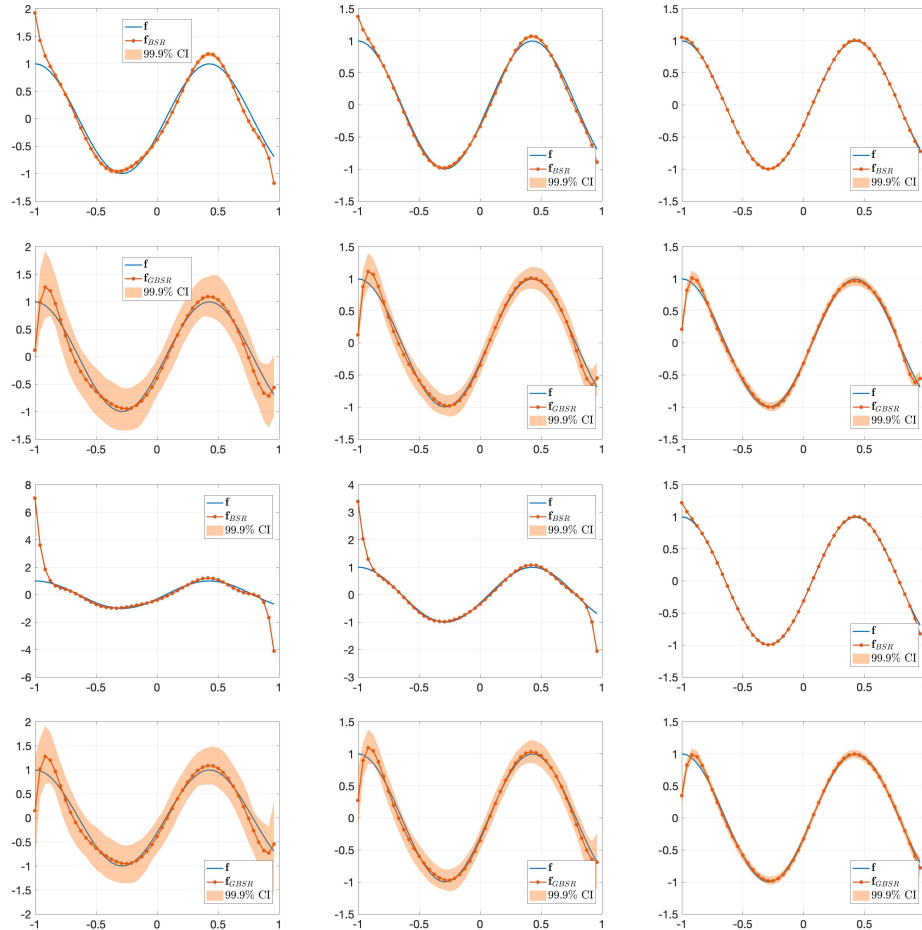


Figure 6.5: Credible intervals with \mathbf{f}_{BSR} and \mathbf{f}_{GBSR} for SNR value 2 (left), 10 (middle) and 30 (left) and $\lambda = 2$ (top and middle-top), $\lambda = 4$ (middle-bottom and bottom).

7. Concluding Remarks. In this investigation we proposed the Bayesian spectral reconstruction (BSR) and generalized Bayesian spectral reconstruction (GBSR) inference methods to recover smooth non-periodic functions from given noisy Fourier data. Both methods are motivated by the theoretical convergence analysis provided for the spectral reconstruction method given noiseless data. These insights are brought into a statistical framework to effectively combine numerical analysis with uncertainty quantification.

The BSR approach provides a statistical framework for the spectral reconstruction method, enabling a better understanding of the limitations for using spectral reconstruction in noisy environments. The likelihood and prior terms follow directly from the error analysis established for the original (noiseless) spectral reconstruction method in [26]. By design, the BSR yields estimates similar to the Gegenbauer reconstruction method, while also providing uncertainty quantification for fixed hyperparameters. As both the likelihood and prior terms are related to Gegenbauer polynomials, the approach limits the space of possible solutions, resulting in very narrow credible intervals. Furthermore, the approximation quality for both spectral reconstruction and BSR rapidly deteriorate with decreasing SNR.

The GBSR approach is then proposed to expand the space of possible solutions, which is accomplished by incorporating the Fourier data directly into the likelihood term (as opposed to first transform-

ing the data to the space of m th-degree Gegenbauer polynomials). In this regard the GBSR provides a more natural construction for computational linear inverse problems. The resulting approximation is more robust with respect to the Gegenbauer polynomial weighting parameter λ , especially in low SNR environments. By design it cannot achieve the same accuracy for high SNR, as the error from the likelihood term is still large due to the effects of the Gibbs phenomenon. The best accuracy for the limiting case of no noise is already obtained using spectral reprojection.

There are clearly benefits and drawbacks in using both the BSR and GBSR, depending on SNR and Gegenbauer weight λ . Importantly, these benefits and drawbacks are highly predictable by the construction of each method and theoretical motivation in [26] (along with the well-known properties of Fourier reconstruction for non-periodic functions). Because of this, developing a hybrid approach that does not require additional user inputs is completely attainable.

Acknowledgements. The authors would like to thank Guohui Song and Jack Friedman for their thoughtful insights during the early stages of this research.

REFERENCES

- [1] M. ABRAMOWITZ AND I. A. STEGUN, *Handbook of Mathematical Functions with Formulas, Graphs and Mathematical Tables*, United States Department of Commerce, 1964.
- [2] B. ADCOCK AND A. C. HANSEN, *Stable reconstructions in hilbert spaces and the resolution of the Gibbs phenomenon*, Appl. Comput. Harmon. Anal., 32 (2012), pp. 357–388.
- [3] R. ARCHIBALD, K. CHEN, A. GELB, AND R. RENAUT, *Improving tissue segmentation of human brain mri through preprocessing by the gegenbauer reconstruction method*, NeuroImage, 20 (2003), pp. 489–502, [https://doi.org/10.1016/S1053-8119\(03\)00260-X](https://doi.org/10.1016/S1053-8119(03)00260-X).
- [4] R. ARCHIBALD AND A. GELB, *A method to reduce the Gibbs ringing artifact in mri scans while keeping tissue boundary integrity*, IEEE Medical Imaging, 21 (2002), pp. 05–319.
- [5] R. ARCHIBALD AND A. GELB, *Reducing the effects of noise in image reconstruction*, Journal of Scientific Computing, 17 (2002), pp. 167–180.
- [6] R. ARCHIBALD, A. GELB, AND R. PLATTE, *Image reconstruction from undersampled fourier data using the polynomial annihilation transform*, Journal of Scientific Computing, (2015), <https://doi.org/10.1007/s10915-015-0088-2>.
- [7] H. BATEMAN, *Higher Transcendental Functions*, vol. 2, McGraw-Hill, New York, 2013.
- [8] A. BECK, *First-Order Methods in Optimization*, SIAM, 2017.
- [9] A. BECK AND M. TEOULLE, *A fast iterative shrinkage-thresholding algorithm for linear inverse problems*, SIAM Journal on Imaging Sciences, 2 (2009), pp. 183–202.
- [10] J. P. BOYD, *Chebyshev and Fourier Spectral Methods*, Dover, 2001.
- [11] J. P. BOYD, *Trouble with gegenbauer reconstruction for defeating gibbs phenomenon: Runge phenomenon in the diagonal limit of gegenbauer polynomial approximations*, Journal of Computational Physics, 204 (2005), pp. 253–264.
- [12] D. CALVETTI, A. PASCARELLA, F. PITOLLI, E. SOMERSALO, AND B. VANTAGGI, *A hierarchical Krylov–Bayes iterative inverse solver for MEG with physiological preconditioning*, Inverse Problems, 31 (2015), p. 125005.
- [13] D. CALVETTI, F. PITOLLI, E. SOMERSALO, AND B. VANTAGGI, *Bayes meets Krylov: Statistically inspired preconditioners for CGLS*, SIAM Review, 60 (2018), pp. 429–461.
- [14] D. CALVETTI, M. PRAGLIOLA, E. SOMERSALO, AND A. STRANG, *Sparse reconstructions from few noisy data: analysis of hierarchical Bayesian models with generalized gamma hyperpriors*, Inverse Problems, 36 (2020), p. 025010.
- [15] D. CALVETTI, E. SOMERSALO, AND A. STRANG, *Hierarchical Bayesian models and sparsity: ℓ_2 -magic*, Inverse Problems, 35 (2019), p. 035003.
- [16] M. CETIN AND R. L. MOSES, *SAR imaging from partial-aperture data with frequency-band omissions*, in Defense and Security, International Society for Optics and Photonics, 2005, pp. 32–43.
- [17] M. L. D. DONOHO AND J. PAULY, *Sparse mri: The application of compressed sensing for rapid mr imaging*, Magnetic Resonance in Medicine, 58 (2007), pp. 1182–1195.
- [18] A. GELB AND Z. JACKIEWICZ, *Determining analyticity for parameter optimization of the gegenbauer reconstruction method*, SIAM Journal on Scientific Computing, 27 (2006), pp. 1014–1032.
- [19] A. GELB AND E. TADMOR, *Detection of edges in spectral data*, Applied and Computational Harmonic Analysis, 7 (1999), pp. 101–135.

- [20] A. GELB AND J. TANNER, *Robust reprojection methods for the resolution of the gibbs phenomenon*, Applied and Computational Harmonic Analysis, 20 (2006), pp. 3–25.
- [21] A. GELMAN, J. CARLIN, H. STERN, AND D. RUBIN, *Bayesian Data Analysis, Second Edition*, Chapman & Hall/CRC Texts in Statistical Science, Taylor & Francis, 2003, <https://books.google.com/books?id=TNyhmkXQSjAC>.
- [22] J. GLAUBITZ, A. GELB, AND G. SONG, *Generalized sparse bayesian learning and application to image reconstruction*, SIAM/ASA Journal on Uncertainty Quantification, 11 (2023), pp. 262–284.
- [23] L. A. GORHAM AND L. J. MOORE, *SAR image formation toolbox for MATLAB*, in Algorithms for Synthetic Aperture Radar Imagery XVII, vol. 7699, SPIE, 2010, pp. 46–58.
- [24] D. GOTTLIEB AND S. ORSZAG, *Numerical analysis of spectral methods: theory and applications*, Society for Industrial and Applied Mathematics, 1977.
- [25] D. GOTTLIEB AND C.-W. SHU, *On the Gibbs phenomenon and its resolution*, SIAM Review, 39 (1997), pp. 644–668, <https://doi.org/10.1137/S0036144596301390>.
- [26] D. GOTTLIEB, C.-W. SHU, A. SOLOMONOFF, AND H. VANDEVEN, *On the Gibbs phenomenon. I. Recovering exponential accuracy from the Fourier partial sum of a nonperiodic analytic function*, J. Comput. Appl. Math., 43 (1992), pp. 81–98, [https://doi.org/10.1016/0377-0427\(92\)90260-5](https://doi.org/10.1016/0377-0427(92)90260-5), [http://dx.doi.org/10.1016/0377-0427\(92\)90260-5](http://dx.doi.org/10.1016/0377-0427(92)90260-5). Orthogonal polynomials and numerical methods.
- [27] L. HE AND L. CARIN, *Exploiting structure in wavelet-based bayesian compressive sensing*, IEEE Transactions on Signal Processing, 57 (2009), pp. 3488–3497.
- [28] J. HESTHAVEN, S. GOTTLIEB, AND D. GOTTLIEB, *Spectral Methods for Time Dependent Problems*, Cambridge University Press, 2007.
- [29] C. V. JAKOWATZ, D. E. WAHL, P. H. EICHEL, D. C. GHIGLIA, AND P. A. THOMPSON, *Spotlight-mode synthetic aperture radar: a signal processing approach*, Springer Science & Business Media, 2012.
- [30] S. JI, Y. XUE, AND L. CARIN, *Bayesian compressive sensing*, IEEE Transactions on Signal Processing, 56 (2008), pp. 2346–2356.
- [31] J. KAIPIO AND E. SOMERSALO, *Statistical and Computational Inverse Problems*, vol. 160, Springer Science & Business Media, 2006.
- [32] P. W. LAUD, *Bayesian statistics: An introduction, second edition. peter m. lee, arnold, 1997. no. of pages: xii+344. price: £19.99. isbn 0-340-67785-6*, Statistics in Medicine, 18 (1999), pp. 2812–2813, <https://api.semanticscholar.org/CorpusID:121074750>.
- [33] R. L. MOSES, L. C. POTTER, AND M. CETIN, *Wide-angle SAR imaging*, in Defense and Security, International Society for Optics and Photonics, 2004, pp. 164–175.
- [34] A. B. OWEN, *Monte Carlo theory, methods and examples*, <https://artowen.su.domains/mc/>, 2013.
- [35] J. G. PIPE AND P. MENON, *Sampling density compensation in MRI: Rationale and an iterative numerical solution*, Magnetic Resonance in Medicine, 41 (1999), pp. 179–186, [https://doi.org/10.1002/\(SICI\)1522-2594\(199901\)41:1<179::AID-MRM25>3.0.CO;2-V](https://doi.org/10.1002/(SICI)1522-2594(199901)41:1<179::AID-MRM25>3.0.CO;2-V), [http://dx.doi.org/10.1002/\(SICI\)1522-2594\(199901\)41:1<179::AID-MRM25>3.0.CO;2-V](http://dx.doi.org/10.1002/(SICI)1522-2594(199901)41:1<179::AID-MRM25>3.0.CO;2-V).
- [36] Y. SAAD, *Iterative Methods for Sparse Linear Systems*, SIAM, 2003.
- [37] B. D. SHIZGAL AND J.-H. JUNG, *Towards the resolution of the gibbs phenomena*, J. Comput. Appl. Math., 161 (2003), pp. 41–65.
- [38] A. SOLOMONOFF, *Reconstruction of a discontinuous function from a few fourier coefficients using bayesian estimation*, J. Sci. Comput., 10 (1995), pp. 29–80.
- [39] W. STEFAN, A. VISWANATHAN, A. GELB, AND R. RENAUT, *Sparsity enforcing edge detection method for blurred and noisy fourier data*, Journal of Scientific Computing, 50 (2012), pp. 536–556.
- [40] A. N. TIKHONOV, A. GONCHARSKY, V. STEPANOV, AND A. G. YAGOLA, *Numerical Methods for the Solution of Ill-Posed Problems*, vol. 328 of Mathematics and Its Applications, Springer Science & Business Media, 2013.
- [41] H. VANDEVEN, *Family of spectral filters for discontinuous problems*, J. Sci. Comput., 6 (1991), pp. 159–192.
- [42] A. VISWANATHAN, A. GELB, D. COCHRAN, AND R. RENAUT, *On reconstruction from non-uniform spectral data*, J. Sci. Comput., 45 (2010), pp. 487–513, <http://dx.doi.org/10.1007/s10915-010-9364-3>.
- [43] S. J. WRIGHT, *Coordinate descent algorithms*, Mathematical Programming, 151 (2015), pp. 3–34.